Spin-orbit torque switching of ultralarge-thickness ferrimagnetic GdFeCo

Niklas Roschewsky, Charles-Henri Lambert, and Sayeef Salahuddin

Phys. Rev. B **96**, 064406 — Published 4 August 2017

DOI: 10.1103/PhysRevB.96.064406

Spin-Orbit Torque Switching of Ultra Large Thickness Ferrimagnetic GdFeCo

Niklas Roschewsky,[1] Charles-Henri Lambert,[2] and Sayeef Salahuddin[2,3,*]

[1] *Department of Physics, University of California, Berkeley, California 94720, USA*
[2] *Department of Electrical Engineering and Computer Sciences, University of California, Berkeley, California 94720, USA*
[3] *Materials Science Division, Lawrence Berkeley National Laboratory, Berkeley, California 94720, USA*

(Dated: May 30, 2017)

We report on spin-orbit torque (SOT) measurements in ferrimagnetic $Gd_{21}(Fe_{90}Co_{10})_{79}$ films with bulk perpendicular magnetic anisotropy (PMA) and thicknesses up to 30 nm. The damping-like and field-like torques have been quantified using second harmonic Hall voltage detection. Both torques show an inverse linear dependence on the thickness that is indicative of the interfacial nature of the torques. The spin-Hall angle remains constant over the thickness range of 10 nm to 30 nm $Gd_{21}(Fe_{90}Co_{10})_{79}$. Remarkably, we find that this interfacial torque is able to switch a 30 nm thick $Gd_{21}(Fe_{90}Co_{10})_{79}$ film with a reasonably large thermal stability of $\approx$100 k_BT.

I. INTRODUCTION

Spin-orbit torque (SOT) devices have received attention recently due to their potential impact on next generation memory technology[1,2]. Here SOT refers to the generation of a non-equilibrium spin-accumulation at a heavy metal (HM)/ferromagnet (FM) interface, either due to the bulk spin-Hall effect in the HM[3,4] or the Rashba-Edelstein effect at the HM/FM interface[5]. This non-equilibrium spin-accumulation diffuses into the ferromagnet[6], where it can reverse the magnetic order via the spin-transfer torque mechanism[7,8].

In most SOT studies, as of today, transition metal magnets, such as Co or Fe with MgO capping layers, are used[9]. Here, the perpendicular magnetic anisotropy (PMA) originates from hybridization effects at the ferromagnet/oxide interface[10]. Due to the inherent interfacial nature of this anisotropy, the ferromagnetic films must be grown very thin (on the order of a 1 nm)and the Co/MgO must be clean and have the right oxygen stoichiometry. This imposes a fundamental bottleneck on the scaling of SOT devices, because it results in a reduction of thermal stability if the area of these devices is reduced.

One way to overcome this problem is to use magnetic materials with bulk PMA[11], where the effect of decreasing footprint area can be compensated by increasing the thickness of the magnet. Indeed, SOT switching has recently been investigated in HM/ferrimagnet structures with bulk PMA, where the ferrimagnets are transition metal (TM)-rare earth (RE) alloys[12–18].

So far, however, a detailed study of the thickness dependence of SOT in magnets with bulk PMA is still lacking in literature. Such a study is important for two reasons: first, the thickness dependence of the torque components can shed light onto the underlying physics of SOT itself; secondly, the thickness dependence of the film is relevant for memory applications, due to the potential for scaling. It should be noted that previous studies on the thickness dependence of SOT in magnets with bulk PMA were limited to ultra thin magnetic films of just a few nanometers thickness due to changes in the crystalline structure with thickness[19].

In the work presented here, we have investigated the thickness dependence of SOT in ferrimagnetic $Gd_{21}(Fe_{90}Co_{10})_{79}$ films. We vary the thicknesses from 10 nm to 30 nm and show that all films can be switched with 200 µs current pulses through adjacent HM layers. To measure the effective magnetic field due to SOT we perform harmonic Hall measurements. The effective field is found to be inversely proportional to the ferrimagnet film thickness and saturation magnetization. In addition, field switching experiments are performed to measure the thermal stability. It is found that the critical switching current j_c, as well as the thermal stability Δ, increase linearly with thickness, so that the switching efficiency j_c/Δ is constant.

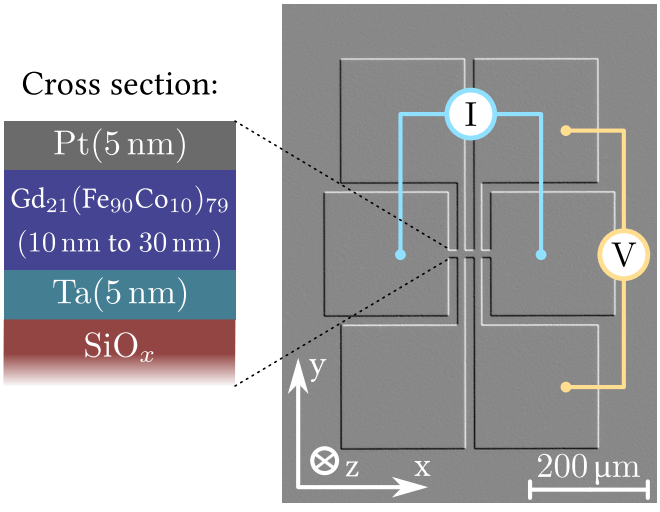

FIG. 1. Microscope image of a Hall bar device. Transition metal rich Ta(5)/$Gd_{21}(Fe_{90}Co_{10})_{79}(t)$/Pt(5) (thickness in nm) structures are investigated. A current is applied along the x-direction and the Hall voltage is detected along the y-direction. The width of the Hall bar is 20 µm.

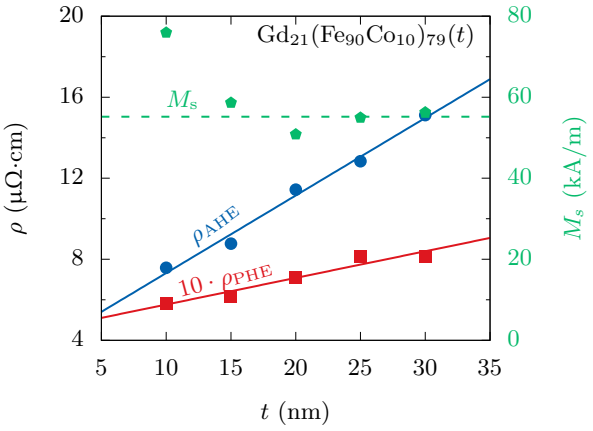

FIG. 2. The AHE resistivity ρ_{AHE} (blue, left axis) as well as the PHE resistivity ρ_{PHE} (red, left axis) depend linearly on the $Gd_{21}(Fe_{90}Co_{10})_{79}$ thickness. The saturation magnetization was measured with VSM magnetometry and is plotted in green on the right axis. M_S is constant for samples with thickness $t > 10\,nm$. At $t = 10\,nm$, the magnetization is enhanced.

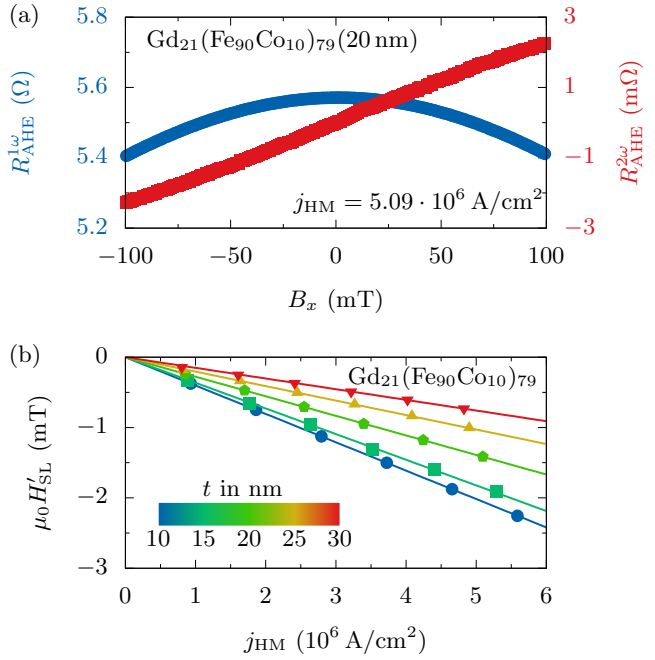

FIG. 3. Harmonic Hall measurement of the effective magnetic field induced by SOT. Panel (a) shows the first- and second harmonic Hall resistance as a function of in-plane magnetic field B_x parallel to the current direction for a 20 nm thick $Gd_{21}(Fe_{90}Co_{10})_{79}$ film. From this measurement the Slonczewski effective field $\mu_0 H_{SL}$ can be extracted. Panel (b) shows that $\mu_0 H'_{SL}$ depends linearly on the current density in the heavy metal in all films under investigation. $\mu_0 H'_{SL}$ is plotted as measured and not corrected for the planar Hall effect in this figure.

II. SAMPLE PREPARATION

We deposited a series of Ta(5)/$Gd_{21}(Fe_{90}Co_{10})_{79}(t)$/Pt(5) films (thickness in nm) on thermally oxidized silicon substrates by RF magnetron sputtering. The thickness t was varied from 10 nm to 30 nm in steps of 5 nm. The base pressure during deposition was below $1 \cdot 10^{-8}$ Torr. After deposition, Hall bar mesa structures were defined by optical lithography and Ar-ion milling. Figure 1 shows an optical image of a typical Hall bar device and the measurement geometry. The width of the Hall bar is 20 µm. A current is applied along the x-direction to excite SOT dynamics. The response of the magnet is detected by the AHE, measured perpendicular to the current direction, along y. Note that $Gd_{21}(Fe_{90}Co_{10})_{79}$ is a transition metal rich alloy with $|m_{TM}| > |m_{RE}|$. The resistivity of the $Gd_{21}(Fe_{90}Co_{10})_{79}$ is $\rho = 1.19\,m\Omega\,cm$.

III. RESULTS AND DISCUSSION

$Gd_{21}(Fe_{90}Co_{10})_{79}$ is a TM-RE alloy, with antiferromagnetic coupling between the TM and RE magnetic moments[20]. The anomalous Hall effect (AHE) in TM-RE ferrimagnets is proportional to the out-of-plane component of the TM magnetization, while the RE magnet does not contribute significantly the the AHE[21,22]. This is because the conduction electrons in the TM are spin polarized while the RE has no spin-split conduction band.

The AHE resistivity ρ_{AHE} as a function of thickness t is shown in Fig. 2, on the left axis. ρ_{AHE} is proportional to the magnetic volume, and thus a linear trend can be observed. In addition, the planar Hall effect (PHE) resistivity ρ_{PHE} was measured. ρ_{PHE} also follows a linear trend, however, ρ_{PHE} is two order of magnitude smaller than ρ_{AHE}. The ratio of AHE and PHE is $\xi = \rho_{PHE}/\rho_{AHE} \approx 3.2\,\%$. The right axis of Fig. 2 shows the saturation magnetization M_s as a function of thickness. M_s is constant for all samples with $t > 10\,nm$. However, the thinnest sample of this series with $t = 10\,nm$ has a larger M_s. We attribute this increase in M_s to a small shift in composition.

To characterize the SOT in our samples we performed harmonic Hall measurements of the effective magnetic fields, following Hayashi *et al.*[23]. We start by measuring the first and second harmonic voltage responses $V_{1\omega}$ and $V_{2\omega}$ to an AC current with $\omega = 1.2\,kHz$ as a function of in-plane magnetic field $B_{x,y}$. To measure the Slonczewski field H_{SL}, the in-plane magnetic field B_x is applied along the x-direction, while the in-plane magnetic field B_y is applied along the y-direction to measure the field-like field H_{FL}. For all harmonic Hall measurements discussed in the following, the samples were magnetized along the $+z$-direction and thus $m_{tot} > 0$.

A typical harmonic Hall measurement to determine

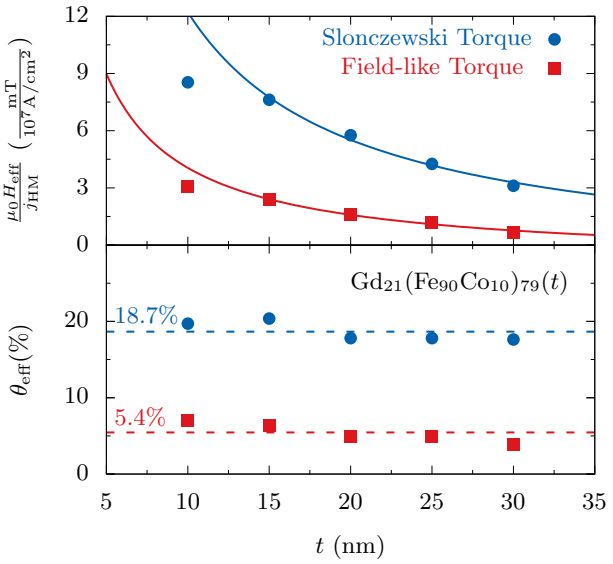

FIG. 4. The upper panel shows the spin torque efficiency as a function of thickness. We find that both the damping-like (blue dots) and the field-like (red squares) torque efficiency decreases linearly with thickness. The lower panel shows the extracted spin Hall angle $\theta_{\rm SH}$ for the thickness series. Since the thickness t was varied but the HM layers were kept unchanged (and thus the HM/FM interface is constant), the effective spin Hall angle does not depend on the thickness of the FM.

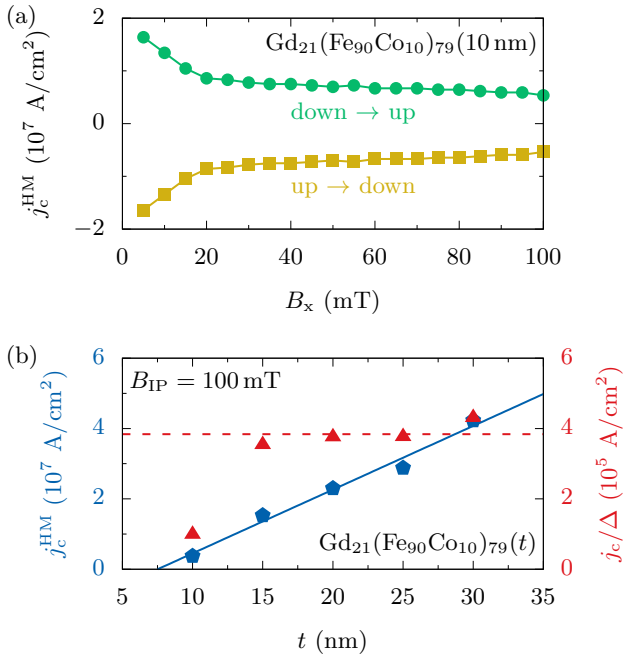

FIG. 5. Panel (a) shows the switching phase diagram for a $\rm Gd_{21}(Fe_{90}Co_{10})_{79}$ film with thickness $t = 10\,$nm. Panel (b) shows that the critical switching current density depends linearly on the film thickness (blue diamonds, left axis). The ratio j_c/Δ is constant for samples with $t > 10\,$nm (red triangles, right axis).

$H_{\rm SL}$ is shown in Fig. 3(a) for a $\rm Gd_{21}(Fe_{90}Co_{10})_{79}$ sample with $t = 20\,$nm and $m_{\rm tot} > 0$. The first harmonic response $R^{1\omega}_{\rm AHE} = V_{1\omega}/I_{\rm FM}$ (blue) follows a quadratic trend as a function of the in-plane magnetic field B_x, while the second harmonic response $R^{2\omega}_{\rm AHE} = V_{2\omega}/I_{\rm FM}$ (red) can be approximated by a linear function of B_x. Here $I_{\rm FM}$ is the current through the $\rm Gd_{21}(Fe_{90}Co_{10})_{79}$.

To compute the effective Slonczewski field from this measurement, the slope of $R^{2\omega}_{\rm AHE}$ is divided by the curvature of $R^{1\omega}_{\rm AHE}$[23]:

$$\mu_0 H'_{\rm SL,FL} = \left(\frac{\partial R^{2\omega}_{\rm AHE}}{\partial B_{x,y}}\right) \times \left(\frac{\partial^2 R^{\omega}_{\rm AHE}}{\partial B^2_{x,y}}\right)^{-1} \qquad (1)$$

Figure 3(b) shows that the effective magnetic field $\mu_0 H'_{\rm SL}$ obtained from this analysis is proportional to the current density in the HM layer in all samples under investigation. This confirms that the effect measured here is indeed caused by SOT, and not by non-linear effects such as heating. In the following, we will refer to the effective field per unit current density through the HM layers as $\zeta_{\rm SL,FL}$.

To account for a mixing of $H'_{\rm SL}$ and $H'_{\rm FL}$ due to the presence of the PHE, the following correction is applied to the data shown in Figure 3[23]:

$$H_{\rm SL,FL} = -2\frac{H'_{\rm SL,FL} + 2\xi H'_{\rm FL,SL}}{1 - 4\xi^2}\,. \qquad (2)$$

Here, ξ is the ratio of PHE resistivity and AHE resistivity: $\xi = \rho_{\rm PHE}/\rho_{\rm AHE}$ and the sample is magnetized upwards ($m_{\rm tot} > 0$). The resulting fields $\zeta_{\rm SL,FL}$ are plotted in the upper panel of Fig. 4 as a function of $\rm Gd_{21}(Fe_{90}Co_{10})_{79}$ thickness. All samples with $t > 10\,$nm, follow a $1/t$ dependence. This is consistent with an interfacial torque of the form:

$$\boldsymbol{\tau}_{\rm SOT} = \frac{\hbar}{2e}\frac{j_{\rm s}}{M_{\rm s} t}\boldsymbol{m} \times (\boldsymbol{\sigma} \times \boldsymbol{m})\,, \qquad (3)$$

where e is the electric charge, $\hbar$ Planck's constant and j_s the spin current. The sample with $t = 10\,$nm does not follow the trend because $M_{\rm s}$ is larger (*c. f.* Fig. 2) and thus $H_{\rm SL,FL}$ is smaller.

Next we use the results for $\zeta_{\rm SL,FL}$ to calculate the spin-Hall angle $\theta_{\rm SH}$ according to:

$$\theta_{\rm SH} = \frac{2|e|}{\hbar} M_{\rm s} t_{\rm FM} \frac{\mu_0 H_{\rm SL,FL}}{j_{\rm HM}}\,. \qquad (4)$$

Here perfect interface transparency was assumed. Figure 4 shows that $\theta_{\rm SH}$ does not depend on t. This is expected, because the SHA only depends on the choice of

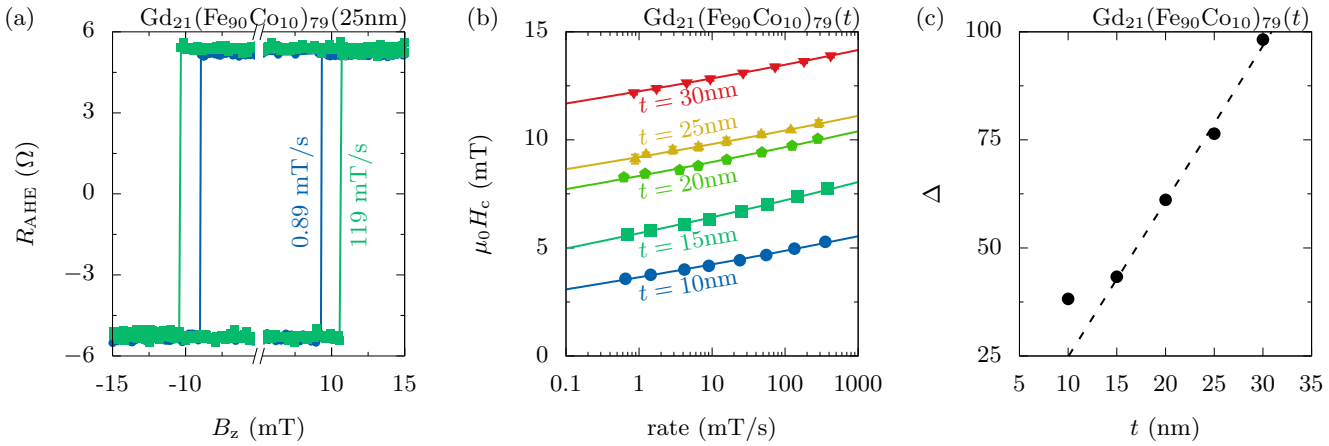

FIG. 6. Measurement of the thermal stability Δ. Panel (a) shows typical hysteresis loops for the films under investigation. B_z is applied along the easy axis of the magnet. The coercive field $\mu_0 H_C$ is increasing with the sweep rate of the magnetic field due to the thermal nature of the switching events. Panel (b) shows the dependence of $\mu_0 H_C$ on the magnetic field sweep rate. The solid lines are fits to the Chantrell model, which is used to determine the thermal stability factor Δ. The extracted values for Δ are plotted in panel (c) as a function of $Gd_{21}(Fe_{90}Co_{10})_{79}$ thickness.

SH metal and the interface. Both did not change upon increasing the $Gd_{21}(Fe_{90}Co_{10})_{79}$ thickness. The average value for the SHA is $\theta_{SH} = 18.7\,\%$. This value is well in agreement with literature values in Pt/Co/Ta systems[24].

In addition to harmonic Hall measurements, we also conducted SOT switching experiments to measure the scaling of critical switching current. To this end, 200 µs long current pulses were applied through the heavy metal layers and the magnetic response was measured by the AHE in the $Gd_{21}(Fe_{90}Co_{10})_{79}$. In order to switch a magnetic film with PMA, an additional magnetic field B_x need to be applied in the x-direction to break the symmetry[25,26]. First we investigated, how the critical current that is needed to switch the magnet, scales with B_x. A typical switching phase diagram for a $Gd_{21}(Fe_{90}Co_{10})_{79}$ film with $t = 10\,\text{nm}$ is shown in Fig. 5(a). As expected, the critical current decreases with increasing B_x. It was further confirmed, that the switching direction is reversed when we change the sign of the in-plane magnetic field[27].

Next we show that the critical current density for SOT-switching j_c at fixed $B_x = 100\,\text{mT}$ scales linearly with t (blue pentagons in Fig. 5(b)). This is expected from macro spin simulations if $B_x < \mu_0 H_k$[28], where H_k is the anisotropy field. The magnitude of j_c is similar to previous results in GdFeCo[15].

Magnetic memory applications require not only low switching current densities but also high thermal stability $\Delta = E_B/k_B T$, where E_B is the activation energy barrier. To investigate the scaling behavior of Δ with t we performed field-switching experiments with an external magnetic field B_z applied along the magnetic easy axis. Field switching is a thermally activated process. Thus, it is expected that the coercive field H_c depends on the rate at which the magnetic field is changed. This is shown in Fig. 6(a), where two hysteresis loops, recorded at different sweep rates, are shown. At slow sweeping rates, the switching event occurs at smaller fields, as it is more likely to thermally nucleate a domain, which will then propagate in the magnet.

The dependence of H_c on the sweeping rate has been studied systematically over 3 orders of magnitude on samples with different GdFeCo thickness. The result is shown in Fig. 6(b): In a semilogarithmic plot H_c depends approximately linearly on the sweeping rate. Note that each value for H_c is the average value from 20 consecutive field switching measurements. To analyze this data we use a model proposed by El-Hilo *et al.*[29]:

$$H_c = H_k \left(1 - \sqrt{\frac{1}{\Delta} \ln\left[\frac{f_0 H_k}{2\Delta}\frac{1}{r}\right]}\right) . \qquad (5)$$

Here, H_k is the anisotropy field, Δ is the thermal stability factor, $f_0 = 1 \cdot 10^{11}\,\text{GHz}$ the attempt frequency and r the sweeping rate. Figure 6(b) shows that this model (solid lines) fits the experimental data well. The extracted values for Δ are shown in Fig. 6(c). For the extraction we assumed an attempt frequency of $f_0 = 1 \cdot 10^{10}\,\text{Hz}$.

A linear trend is seen in Fig. 6(c) because the thermal stability is proportional to the magnetic volume. The sample with $t = 10\,\text{nm}$ does not follow the trend, which we attribute again to an increase in saturation magnetization.

The switching efficiency for SOT devices is defined as j_c/Δ. In our devices, j_c as well as Δ scale linearly with thickness. Thus, the switching efficiency does not depend on the thickness as shown in Fig. 5(b) on the right axis (red triangles).

All results discussed to far have been obtained on $Gd_x(Fe_{90}Co_{10})_{100-x}$ samples with $x = 21\,\%$. However, it is known that the magnetic properties of TM-RE alloys

change drastically with composition[30]. In fact, previous experiments have shown that SOT exhibit a distinctive dependence on the film composition[14–17]. So far the composition dependence has only been studied in very thin films with $t \leq 5\,\mathrm{nm}$. Further, the effective fields were estimated from domain wall motion experiments[31]. Here we used harmonic Hall measurements to characterize the composition dependence of the effective SOT fields in 30 nm thick $Gd_x(Fe_{90}Co_{10})_{100-x}$ films.

Following eqn. (3), we expect the effective magnetic field to diverge at the magnetization compensation point, since M_s will vanish. This trend can clearly be seen in Fig. 7, where we plot $\mu_0 H_{SL,FL}/j_{HM}$ vs. the concentration x for the damping-like field as well as for the field-like field.

Next, we calculate θ_{eff}, using the values obtained for $\mu_0 H_{eff}/j_{HM}$. Figure 7 shows that θ_{eff} is approximately constant, since only the composition x but not the SH metal or the interfaces were changed. The average value for the SHA is $\theta_{eff} = 18.5\,\%$. This value is well in agreement with the value of θ_{eff} reported in Fig. 4.

IV. CONCLUSION

In conclusion, we showed that the effective magnetic field $H_{SL,FL}$, induced by SOT, scales as $H_{SL,FL} \propto M_s^{-1} t_{FM}^{-1}$ for all samples under investigation in this study. This indicates that the torques are interfacial in nature. θ_{SH} is found to be constant at an average value of $\theta_{SH} = 18\,\%$. We have also shown that $Gd_{21}(Fe_{90}Co_{10})_{79}$ as thick as 30 nm can be switched with SOT currents. j_c, as well as Δ were found to scale linearly with thickness, keeping the switching efficiency j_c/Δ constant. Thus our work, together with torque and thermal stability measurements as a function of thickness, provides a self-consistent picture of how the SOT scales in ferrimagnet/heavy metal heterostructures. The ability to switch large thickness ferrimagnets with high thermal stability might have important implications for future magnetic-memory applications.

ACKNOWLEDGMENT

We thank Johannes Mendil and Samuel Smith for fruitful discussions. This work was supported by the Office of Science, Office of Basic Energy Sciences, Materials Science and Engineering Division and the U.S. Department of Energy under Contract No. DE-AC02-05-CH11231 within the NEMM program (KC2204). Device fabrication was supported by the STARNET/FAME Center.

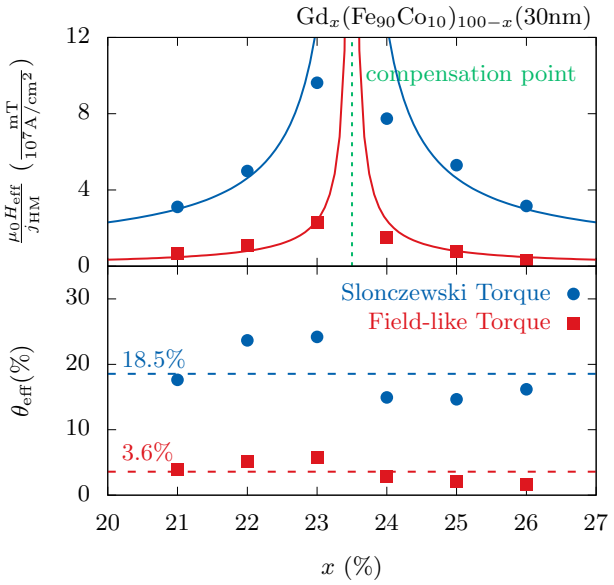

FIG. 7. Upper panel: The spin torque efficiency as a function of film composition x is shown for the $t = 30\,\mathrm{nm}$ sample. The spin torque efficiency diverges close to the compensation point. Lower panel: The effective spin Hall angle θ_{SH} is plotted as a function of composition. θ_{SH} shows no distinct dependence on the composition x, since the HM/FM interface is unaltered.

* sayeef@berkeley.edu

[1] S. W. Lee and K. J. Lee, Proc. IEEE **104**, 1831 (2016).
[2] Y. Fan, P. Upadhyaya, X. Kou, M. Lang, S. Takei, Z. Wang, J. Tang, L. He, L.-T. Chang, M. Montazeri, G. Yu, W. Jiang, T. Nie, R. N. Schwartz, Y. Tserkovnyak, and K. L. Wang, Nat. Mat. **13**, 699 (2014).
[3] L. Liu, C. F. Pai, Y. Li, H. W. Tseng, D. C. Ralph, and R. A. Buhrman, Science **336**, 555 (2012).
[4] L. Liu, O. J. Lee, T. J. Gudmundsen, D. C. Ralph, and R. A. Buhrman, Phys. Rev. Lett. **109**, 96602 (2012).
[5] I. M. Miron, K. Garello, G. Gaudin, P. J. Zermatten, M. V. Costache, S. Auffret, S. Bandiera, B. Rodmacq, A. Schuhl, and P. Gambardella, Nature **476**, 189 (2011).
[6] P. M. Haney, H. W. Lee, K. J. Lee, A. Manchon, and M. D. Stiles, Phys. Rev. B **87**, 174411 (2013).
[7] L. Berger, Phys. Rev. B **54**, 9353 (1996).
[8] J. C. Slonczewski, J. Mag. Mat. **159**, L1 (1996).
[9] S. Ikeda, K. Miura, H. Yamamoto, K. Mizunuma, H. D. Gan, M. Endo, S. Kanai, J. Hayakawa, F. Matsukura, and H. Ohno, Nat. Mat. **9**, 721 (2010).
[10] H. X. Yang, M. Chshiev, B. Dieny, J. H. Lee, A. Manchon, and K. H. Shin, Phys. Rev. B **84**, 54401 (2011).
[11] F. Hellman and E. M. Gyorgy, Physical Review Letters **68**, 1391 (1992).
[12] Z. Zhao, M. Jamali, A. K. Smith, and J. P. Wang, Appl. Phys. Lett. **106**, 132404 (2015).

[13] K. Ueda, C.-F. Pai, A. J. Tan, M. Mann, and G. S. D. Beach, Appl. Phys. Lett. **108**, 232405 (2016).

[14] K. Ueda, M. Mann, C. F. Pai, A. J. Tan, and G. S. D. Beach, Appl. Phys. Lett. **109**, 232403 (2016).

[15] N. Roschewsky, T. Matsumura, S. Cheema, F. Hellman, T. Kato, S. Iwata, and S. Salahuddin, Appl. Phys. Lett. **109**, 112403 (2016).

[16] J. Finley and L. Liu, Phys. Rev. Applied **6**, 54001 (2016).

[17] R. Mishra, J. Yu, X. Qiu, M. Motapothula, T. Venkatesan, and H. Yang, (2017), arXiv:1703.08263.

[18] W. S. Ham, S. Kim, D.-H. Kim, K. J. Kim, T. Okuno, H. Yoshikawa, A. Tsukamoto, T. Moriyama, and T. Ono, (2017), arXiv:1703.00995.

[19] H. R. Lee, K. Lee, J. Cho, Y. H. Choi, C. Y. You, M. H. Jung, F. Bonell, Y. Shiota, S. Miwa, and Y. Suzuki, Sci. Rep. **4**, 6548 (2014).

[20] I. A. Campbell, J Phys F **2**, L47 (1972).

[21] T. Shirakawa, Y. Nakajima, K. Okamoto, S. Matsushita, and Y. Sakurai, AIP Conference Proceedings **34**, 349 (1976).

[22] Y. Mimura, N. Imamura, and Y. Kushiro, J. Appl. Phys. **47**, 3371 (1976).

[23] M. Hayashi, J. Kim, M. Yamanouchi, and H. Ohno, Phys. Rev. B **89**, 144425 (2014).

[24] S. Woo, M. Mann, A. J. Tan, L. Caretta, and G. S. D. Beach, Appl. Phys. Lett. **105**, 212404 (2014).

[25] R. Lo Conte, A. Hrabec, A. P. Mihai, T. Schulz, S.-J. Noh, C. H. Marrows, T. A. Moore, and M. Kläui, Appl. Phys. Lett. **105**, 122404 (2014).

[26] K. Garello, I. M. Miron, C. O. Avci, F. Freimuth, Y. Mokrousov, S. Blugel, S. Auffret, O. Boulle, G. Gaudin, and P. Gambardella, Nat. Nano **8**, 587 (2013).

[27] K. Garello, C. O. Avci, I. M. Miron, M. Baumgartner, A. Ghosh, S. Auffret, O. Boulle, G. Gaudin, and P. Gambardella, Appl. Ph.. L.. **105** (2014), 10.1063/1.4902443, 1310.5586.

[28] K. S. Lee, S. W. Lee, B. C. Min, and K. J. Lee, Appl. Phys. Lett. **102**, 112410 (2013).

[29] M. El-Hilo, A. M. de Witte, K. O'Grady, and R. W. Chantrell, J. Mag. Mat. **117**, L307 (1992).

[30] F. Hellman, Appl. Phys. Lett. **59** (1991).

[31] C. F. Pai, M. Mann, A. J. Tan, and G. S. D. Beach, Phys. Rev. B **93**, 144409 (2016).